



Isomeric Triptycene Triquinones as Universal Cathode Materials for High Energy Alkali Metal Batteries

Hyunji Park^[a, b], Yoshiaki Shuku^[c], Jihyun Lee,^[d] Kyunam Lee,^[a] Dong Joo Min,^[a] Byeong-Kwan An,^[d] Kuino Awaga,^{*[c]} Soo Young Park,^{*[a]} and Ji Eon Kwon^{*[a, b]}

Organic electrode materials have been extensively researched for alkali metal batteries such as Li, Na, and K batteries due to their unique redox mechanism independent of types of charge-carrying ions and flexible intermolecular structures facilitating the insertion of bulky metal-ions. This study presents an *ortho*-isomer of triptycene tribenzoquinone (*o*-TT) as a universal organic cathode material for alkali metal batteries. To elevate the redox potentials of previously reported triptycene tribenzoquinone (TT) without sacrificing its large specific capacity

(~386 mAh g⁻¹), the structural isomers of benzoquinone units in the TT molecule were designed by changing their carbonyl group position from *para*- to *ortho*-position. Due to multi-electron redox reactions and the elevated redox potentials, *o*-TT shows high energy densities of 945, 767, and 597 Wh kg⁻¹ in Li, Na, and K cells, respectively. Finally, its cycle stability is significantly improved by fabricating composite electrodes with disordered mesoporous carbon (DOMC).

Introduction

With the rapid growth of the market for electric vehicles (EV) and portable electronics, it has been essential to develop high energy density batteries with sustainability and low cost.^[1] However, conventional lithium-ion batteries (LIBs) relying on inorganic electrodes such as transition metal oxides have reached their theoretical limit regarding capacity and energy density.^[2] Furthermore, due to the depletion of lithium

resources with uneven geographic distribution, the price of lithium is expected to skyrocket, compelling the development of alternatives.^[3] Among others, sodium-ion (SIBs) and potassium-ion batteries (PIBs) are drawing considerable attention because alkali metals have physicochemical and electrochemical properties similar to lithium but are more abundant.^[4] Nonetheless, the larger size of Na⁺ and K⁺ (ionic radius = 0.76, 1.02, and 1.38 Å for Li⁺, Na⁺, and K⁺, respectively) makes their intercalation process more sluggish than Li⁺ in the rigid crystal structure of inorganic electrode materials, leading to slower rate performance and lower capacity utilization.^[5] Furthermore, the huge structural change in the electrode materials during the charge/discharge process also brings about poor cycle stability of SIBs and PIBs.^[6]

In contrast, organic materials have more flexible crystal structures where each molecule is stacked through weak secondary interactions, including van der Waals forces, π-π interactions, and hydrogen bonds, facilitating the incorporation of large-size ions. Moreover, their redox reactions typically do not rely on the types of counter-ions, which enables universal utilization of the organic electrode materials in diverse metal batteries.^[7]

Particularly, quinone derivatives have attracted much attention because of their high theoretical capacity, structural diversity, and potentially low cost with sustainability.^[8] For example, Chen group reported two macrocyclic compounds composed of multiple quinones as organic cathode materials.^[9] In Li-ion cells, calix[4]quinone(C4Q)^[9a] and pillar[5]quinone(P5Q),^[9b] which bear four and five quinones, respectively, showed high discharge capacities around 420 mAh g⁻¹ at 0.2 C with average discharge potentials of ~2.6 V vs. Li⁺/Li. But, in Na-ion cells, their operating potentials dropped below 2.5 V vs. Na/Na⁺ due to the higher standard reduction potential of Na (~2.70 V vs. SHE) than Li (~3.04 V vs. SHE).^[10]

[a] H. Park,[†] Dr. K. Lee, Dr. D. Joo Min, Prof. S. Young Park, Dr. J. Eon Kwon
Laboratory for Supramolecular Optoelectronic Materials (LSOM)

Department of Materials Science and Engineering
Research Institute of Advanced Materials (RIAM)

Seoul National University

1 Gwanak-ro, Gwanak-gu, Seoul 08826 (Republic of Korea)
E-mail: parksy@snu.ac.kr

[b] H. Park,[†] Dr. J. Eon Kwon

Functional Composite Materials Research Center
Institute of Advanced Composite Materials, Korea Institute of Science and Technology (KIST)
92 Chudong-ro, Bongdong-eup, Wanju-gun, Jeonbuk 55324 (Republic of Korea)

E-mail: jekwon@kist.re.kr

[c] Dr. Y. Shuku,[†] Prof. K. Awaga

Department of Chemistry
Nagoya University
Furo-cho, Chikusa-ku, Nagoya 464-8602 (Japan)
E-mail: awaga.kunio@b mbox.nagoya-u.ac.jp

[d] J. Lee, Prof. B.-K. An

Department of Chemistry
Catholic University of Korea
43 Jibong-ro, Bucheon, Gyeonggi-do, 14662 (Republic of Korea)

^[†] These authors contributed equally to this work.

Supporting information for this article is available on the WWW under
<https://doi.org/10.1002/batt.202200497>

An invited contribution to a Special Collection on Organic Batteries.

© 2022 The Authors. *Batteries & Supercaps* published by Wiley-VCH GmbH.
This is an open access article under the terms of the Creative Commons Attribution Non-Commercial License, which permits use, distribution and reproduction in any medium, provided the original work is properly cited and is not used for commercial purposes.

Meanwhile, poly(anthraquinonyl sulfide) (PAQS) electrode has also been reported for various metal batteries. Despite the use of more diluted electrolyte, PAQS showed a lower average discharge potential in a K-ion cell (~1.85 V vs. K^+/K)^[11] than in a Li-ion cell (~2.1 vs. Li^+/Li)^[12] due to higher reduction potential of K (~2.93 V vs. SHE) than Li. Therefore, for utilizing quinones as electrode materials in such SIBs and PIBs, their molecular structures should be further tailored to compensate for the voltage drop.

So far, the most widely used strategies to elevate the redox potential of organic electrode materials include introducing electron-withdrawing groups^[13] and substituting heteroatoms.^[14] However, despite a rise in charge/discharge voltage, such strategies naturally increase the redox-inactive molecular weight of electrode materials, leading to a significant decrease in their specific capacity.

On the other hand, the Poizot group reported that adjusting the position of carbonyl redox centers in Li_4DHT from *para*-to *ortho*-position in relation to each other led to redox potential elevation of 300 mV without sacrificing its capacity.^[15] Subsequently, using theoretical calculation methods, Chen and colleagues revealed that *ortho*-quinones indeed have higher redox potentials than other quinones due to the stabilization of the lowest unoccupied molecular orbital (LUMO) energy.^[16] Nevertheless, *ortho*-quinones have seldom been evaluated for

electrode materials in alkali metal batteries compared to *para*-quinones.

Previously, we reported a novel quinone electrode material in which a triptycene skeleton covalently connected three *p*-benzoquinones (*p*-BQs), namely triptycene tribenzoquinone (TT, see Figure 1c for its chemical structure).^[17] In a Li cell, TT delivered a high capacity of 387 mAh g⁻¹ relying on reversible five one-electron reductions with an average discharge potential of 2.67 V vs. Li^+/Li . The X-ray single crystal analysis revealed that the unique 3-D molecular structure of TT provided sufficient free volumes for Li-ions to access the carbonyl redox centers efficiently.^[17,18] Such promising properties prompted us to utilize the triptycene quinone as an electrode material for SIBs and PIBs.

Aiming to elevate the redox potential without loss of specific capacity at the same time, we herein employ an isomeric triptycene quinone bearing three *o*-BQs (*o*-TT, see Figure 1d for chemical structure). In comparison with the original TT having *p*-BQs, it is found that *o*-TT shows elevated charge/discharge voltages not only in a Li cell but also in Na and a K cell while maintaining its high specific capacity, suggesting its versatility with high energy density. To optimize the electrochemical performance of the two triptycene quinones in each metal cell, various electrolytes composed of different organic solvents and metal-ion salts are employed. Finally, nanocomposite materials with mesoporous carbon are

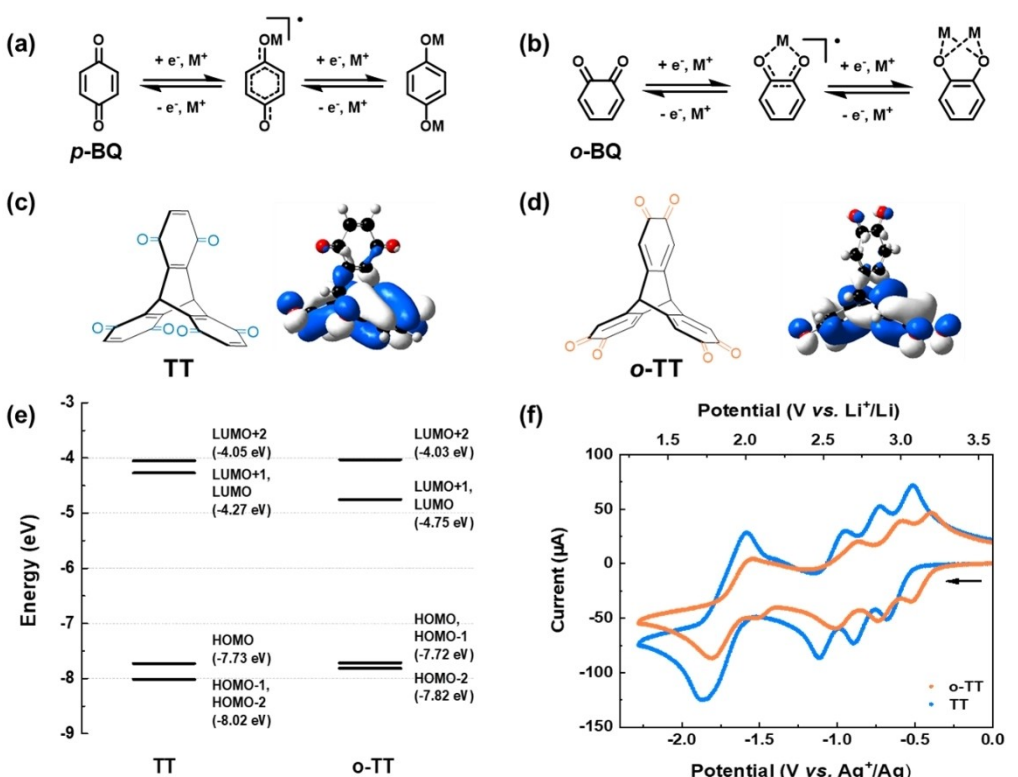


Figure 1. The chemical structures with the reduction reaction schemes for a) *p*-BQ and b) *o*-BQ. The chemical structures and LUMO diagrams of c) TT and d) *o*-TT. e) The calculated frontier molecular orbital (FMO) energies of TT and *o*-TT using the DFT method. HOMO-1 and HOMO-2 stand for the second and the third highest occupied molecular orbital, respectively. LUMO + 1 and LUMO + 2 stand for the second and the third lowest unoccupied molecular orbital, respectively. f) The cyclic voltammogram of 5 mM TT derivatives using an Ag wire in a 0.01 M $Ag/AgNO_3$ solution as a reference electrode. The potential values are linearly rescaled with respect to Li^+/Li by assuming $Fc^+/Fc = 3.25$ V vs. Li^+/Li .^[23]

fabricated to improve the cycle stability of the triptycene quinones.

Results and Discussion

Materials design and electrochemical properties

Typically, benzoquinones, including *p*-BQ and *o*-BQ, undergo two stepwise single-electron reductions (see Figure 1a and b for their reaction schemes). The previously reported TT bears three *p*-BQ units on a triptycene skeleton, and thus it can theoretically store six Li-ions by six reduction reactions to deliver a theoretical specific capacity ($C_{\text{theoretical},6e^-}$) of 467 mAh g⁻¹. To elevate its redox potential, we designed a regioisomer of TT (*o*-TT, see Figure 1d) by switching the position of its carbonyl groups from *para* into *ortho* to each other. TT (9,10-dihydro-9,10[1',2']-benzenoanthracene-1,4,5,8,13,16-hexone) was synthesized according to the reported procedures,^[19] and *o*-TT (9,10-dihydro-9,10-[1,2]benzenoanthracene-2,3,6,7,14,15-hexaone) was prepared by following a reported procedure with a slight modification (see Experimental Section and Figure S1).^[20]

Recently, Chen group elucidated that the redox potential of quinones rose in the order of *para*-<discrete-<*ortho*-quinones based on density functional theory (DFT) calculation indeed results of 20 quinone isomers.^[16] As shown in Figure 1(e), DFT calculation reveals that *o*-TT has lower LUMO energy (-4.75 eV) than TT (-4.27 eV). Since the LUMO energy provides an approximation for the electron affinity (EA) according to Koopman's theorem,^[21] it is anticipated that *o*-TT has a higher reduction potential than TT.^[17] Indeed, the EA values are calculated to be 3.07 and 3.58 eV for TT and *o*-TT, respectively, by the DFT method. The redox potential elevation of *ortho*-quinones is most likely attributed to the energy destabilization induced by repulsion between the two dipolar carbonyl groups in close proximity to each other.^[22] Because *o*-TT has an identical molecular weight to TT, however, its theoretical specific capacity is estimated to remain the same as TT.

To investigate the electrochemical properties of the two triptycene quinones in practice, cyclic voltammetry (CV) was performed in a dimethylformamide (DMF) solution with 0.1 M tetrabutylammonium hexafluorophosphate (TBAHFP) as a supporting electrolyte. The two TT isomers show similar redox curves in shapes (see Figure 1f). Both redox curves consist of three well-separated peaks in the range of -1.2 to -0.5 V vs. Ag⁺/Ag and one large peak in the range of -1.5 to -2.0 V vs. Ag⁺/Ag. The former three peaks correspond to the first reduction of each BQ unit in the TT derivatives, and the latter large peak arises from their respective second reduction (see Figure 1a and b for the reduction reaction schemes). As revealed in the previous study,^[17] from the CV results, it can be inferred that the two TT derivatives are able to be reduced by accepting only five electrons (i.e., three electrons for the first reductions and two electrons for the second reductions of their BQ units, respectively) due to instability of the hexa-anion. But it should be noted that, as expected, *o*-TT shows higher

reduction potentials ($E_{1/2} = -0.45$ V, -0.67 V, -0.94 V, and -1.68 V vs. Ag⁺/Ag) than the original TT ($E_{1/2} = -0.60$ V, -0.81 V, -1.03 V, and -1.72 V vs. Ag⁺/Ag).

Li half-cell test

First, the electrochemical performance of *o*-TT and TT as cathode materials in Li cells was evaluated by fabricating CR2032 coin-type half-cells. We used 2 M lithium bis(trifluoromethanesulfonyl)imide (LiTFSI) in a 1:1 (v/v) mixture of 1,3-dioxolane (DOL) and 1,2-dimethoxyethane (DME) with 1 wt% LiNO₃ for the electrolyte, as TT showed the best performance with this electrolyte in the previous study.^[17] As shown in Figure 2a, in the initial galvanostatic discharge, TT and *o*-TT delivers a specific capacity of 384 and 336 mAh g⁻¹, respectively, at 0.1 C-rate. The current rates were calculated based on the theoretical capacity of each TT ($C_{\text{theoretical},6e^-} = 467$ mAh g⁻¹). Given that the TT derivatives can store only five Li-ions (*vide supra*), it can be deduced that most of their capacities were utilized in the Li cells ($C_{\text{theoretical},5e^-} = 389$ mAh g⁻¹).

In the galvanostatic test, TT shows two well-defined charge/discharge voltage plateaus. The upper plateau corresponds to the first reductions of each *p*-BQ unit of TT, while the lower one corresponds to their respective second reductions (see Figure 1f for comparison). In contrast, *o*-TT exhibits three voltage plateaus. It is found that the profile corresponding to the first reductions of the three *o*-BQ units split into two plateaus composed of a flat and a slopy one. The voltage plateau corresponding to the second reductions also becomes slightly steeper. Nevertheless, it is worth noticing that the plateaus of *o*-TT are located at a higher voltage than the original TT, as anticipated by the DFT calculations and the CV measurements shown above.

The dQ/dV plot (Figure 2c) more clearly shows the voltage difference between TT and *o*-TT in charge/discharge. In the *o*-TT electrode, the first and the second discharge reaction, corresponding to the flat and the upper slopy plateau, peaking at 3.16 V and 3.01 V vs. Li⁺/Li, respectively, which are much higher than the first discharge peak of TT (2.89 V vs. Li⁺/Li). But, the third discharge reaction, corresponding to the lower slopy plateau, shows a similar peak voltage (2.41 V vs. Li⁺/Li) with the second discharge peak of TT (2.46 V vs. Li⁺/Li). Naturally, the average discharge voltage of *o*-TT is elevated up to 2.81 V with a specific energy of 945 Wh kg⁻¹, achieving one of the highest values among reported n-type organic electrodes (Figure 2b and Table S1).

Na half-cell test

Encouraged by the high capacity utilization and voltage elevation of *o*-TT in the Li cells, we applied the two TT derivatives as electrode materials for Na cells. For the electrolyte in the Na cells, we first used 1 M NaTFSI in DOL/DME (1:1 by vol), consisting of identical anion and solvents with the Li-

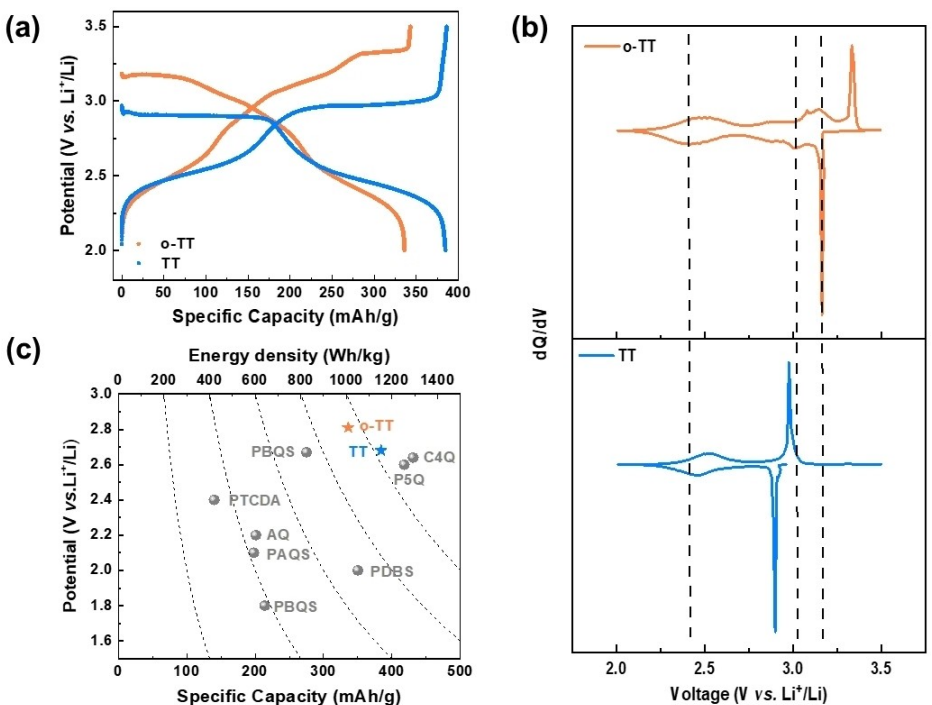


Figure 2. The electrochemical performances of TT and o-TT cathodes in the Li coin cells. a) The initial galvanostatic charge/discharge profiles at 0.1 C-rate, and b) the corresponding differential capacity curves. c) The plot of average voltage vs. specific capacity with the specific energy of representative n-type organic cathodes in the Li cells.

ion electrolyte. However, in the Na cells, unstable charge/discharge profiles were obtained from both materials (see Figure S2), which is attributed to the degradation of the Na metal anode induced by TFSI anion in the ether-based solvent.^[24] Thus, we changed the salt to other anions but kept using the DOL/DME solvent mixture, given that quinone-based electrodes typically exhibited better electrochemical performances in the ether-based electrolytes.^[25]

With 1 M NaPF₆ in DOL/DME (1:1 by vol), both the TT and o-TT electrodes showed stable charge/discharge profiles (Figure S3a and b), but much fewer capacities were utilized than their theoretical specific capacity. However, the initial discharge capacity of o-TT was considerably improved up to 360 mAh g⁻¹ (Figure 3a) by increasing the concentration of NaPF₆ salt from 1 M to 2 M in the DOL/DME 1:1 mixture. In contrast, changing the salt concentration barely affected the performance of TT in the Na cells (Figure S3c). Instead, when we changed the electrolyte solvent from DOL/DME 1:1 mixture to unmixed DME, the TT electrode could deliver better electrochemical performance with a high specific capacity of 357 mAh g⁻¹ (Figure 3a). But o-TT delivered a much low specific capacity in the DME electrolyte (Figure S3d). We also tested 1 M NaClO₄ salts for the electrolytes; however, unstable charge/discharge plateaus with a low specific capacity were obtained from the o-TT electrode (Figure S4). Thus, in this study, the TT derivatives for the Na cells were further evaluated in their respective optimized electrolyte (i.e., 1 M NaPF₆ in DME for TT and 2 M NaPF₆ in DOL/DME (1:1) for o-TT, respectively).

Similar to the Li cell results, the TT electrode shows two distinct discharge voltage plateaus peaking at 2.54 and 2.04 V

vs. Na⁺/Na, respectively, in the Na cell (see Figure 3a and b). In the case of o-TT, three voltage plateaus are also observed in the initial discharge process, similar to the Li cell. The first plateau, corresponding to the first reduction of one of the three quinones in o-TT, locates at a higher voltage than that of TT, as expected. However, it is found that the second plateau, which originates from the first reduction process of the other two quinones in o-TT, occurs at much lower voltages. The two plateaus peak at 2.74 and 2.13 V vs. Na⁺/Na, respectively, as revealed by the differential capacity plot (Figure 3b). Subsequently, the third plateau, corresponding to the second reduction process of the quinones in o-TT, occurs at 1.82 V vs. Na⁺/Na, which is lower than that of TT. Consequently, in the Na cells, o-TT provides a lower average voltage (2.13 V vs. Na⁺/Na) than TT (2.29 V vs. Na⁺/Na), leading to a slight decrease in the specific energy (767 Wh kg⁻¹) than TT (818 Wh kg⁻¹). However, as shown in Figure 3(c), it should be noted that the two TT molecules provide superior specific energy outperforming most n-type organic electrode materials for the Na cells reported so far.

K half-cell test

In the K cells, the two TT derivatives also showed unstable charge/discharge profiles with KTFSI salt (Figure S5), but they are stable with KPF₆. Interestingly, TT performed better in a 1:1 DOL/DME mixture than in an unmixed DME electrolyte (see Figure S6). Then, when we increased the KPF₆ salt concentration in the 1:1 DOL/DME electrolyte to 2 M, the TT electrode

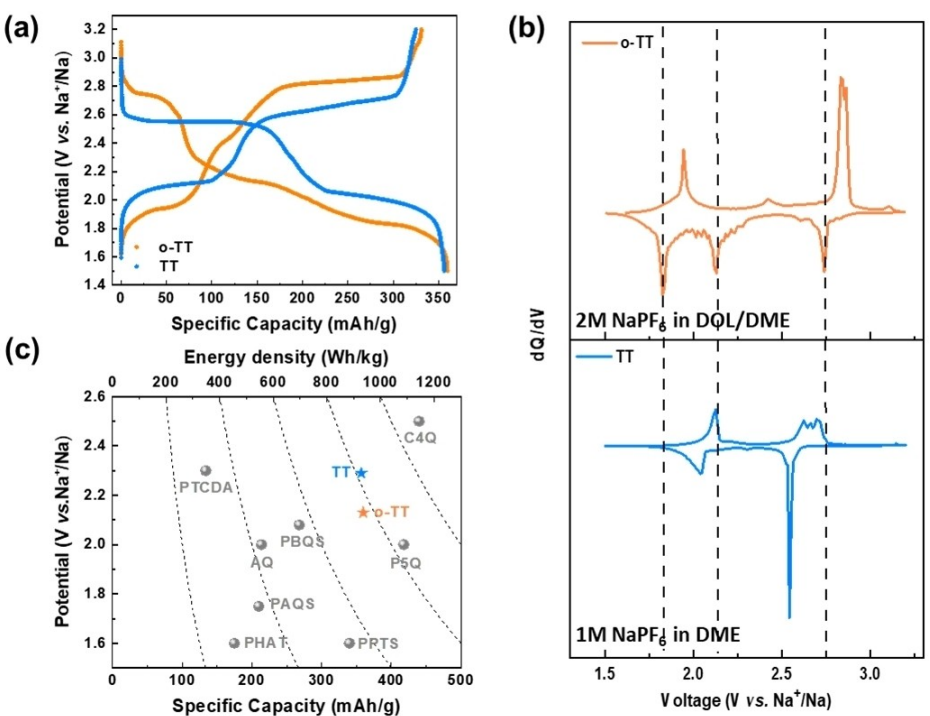


Figure 3. The electrochemical performances of TT and o-TT cathodes in the Na cells. a) The initial galvanostatic charge/discharge profiles at 0.1 C-rate, and b) the corresponding differential capacity analysis curves. c) The plot of average voltage vs. specific capacity with the specific energy of representative n-type organic cathodes in Na cells.

delivered a specific capacity of 280 mAh g⁻¹. In contrast, an electrolyte containing 1 M KPF₆ in DME was more suitable for o-TT. But, increasing the salt concentration of KPF₆ to 2 M was harmful to o-TT, considerably lowering its delivered capacity (Figure S7). In the optimized electrolyte, o-TT delivered a specific capacity of 255 mAh g⁻¹ (Figure 4a).

Similar to the Li and Na cells, TT shows two obvious voltage plateaus corresponding to the first and second reductions of *p*-quinones in TT. In sharp contrast, the charge/discharge profiles of o-TT are much sloppier than the other type cells without a distinct plateau. But the differential analysis clearly indicates two charge/discharge peaks. In a dQ/dV plot, o-TT shows sharp and broad discharge peaks at 2.97 V and 1.98 V vs. K^{+/K}, respectively, while TT has two sharp peaks at 2.92 V and 1.82 V vs. K^{+/K}. Because the higher salt concentration of the electrolyte for TT could lower its redox voltages, we compared the differential capacity curves of the two TTs in the same electrolyte. But, even with 1 M KPF₆ in DME, it is found that o-TT shows higher discharge voltages than TT (Figure S8b). However, the slopy voltage profile of o-TT resulted in a slightly lower average discharge voltage (2.34 V vs. K^{+/K}) than TT (2.39 V vs. K^{+/K}) in their respective optimized electrolyte. Nevertheless, it should be noted that the energy density of o-TT (597 Wh kg⁻¹) and TT (669 Wh kg⁻¹) exceeds most other organic n-type electrode materials in K cells.^[26,27]

Charge/discharge mechanism study

To elucidate the redox mechanism of TT and o-TT in the metal cells, ex-situ FT-IR measurements were carried out at five different states-of-charge (SOCs): the pristine, half-discharged, fully discharged, half-charged, fully-recharged (see points A-E in Figure 5). Figure 5 shows the FT-IR spectra changes with the corresponding charge/discharge profiles in the Li cells. In the pristine electrodes, a stretching vibration peak of carbonyl C=O groups appears at 1657 and 1659 cm⁻¹ for TT and o-TT, respectively.^[28] By discharge, the C=O peak is attenuated, and simultaneously a new peak at 1490 and 1482 cm⁻¹ arises for TT and o-TT, respectively, corresponding to the C–O–Li group at the half-discharge state (point B in Figure 5). It should be noted that the original carbonyl peaks are almost completely diminished, still at the half-discharged state, implying most of the six carbonyl groups in the TT derivatives are already bound with the inserted three Li-ions.

Upon further discharge to point C, the new peaks are slightly red-shifted to 1470 cm⁻¹ for TT and o-TT, respectively, which indicates that the bond length of the enolate carbonyl groups is increased. Thus, it can be inferred that the enolate carbonyl groups should form additional coordination bonds with the subsequently inserted Li-ions in the second discharge step, weakening the bond strength of C–O groups (see Figure S9 for the plausible charge/discharge mechanism of the TT derivatives).

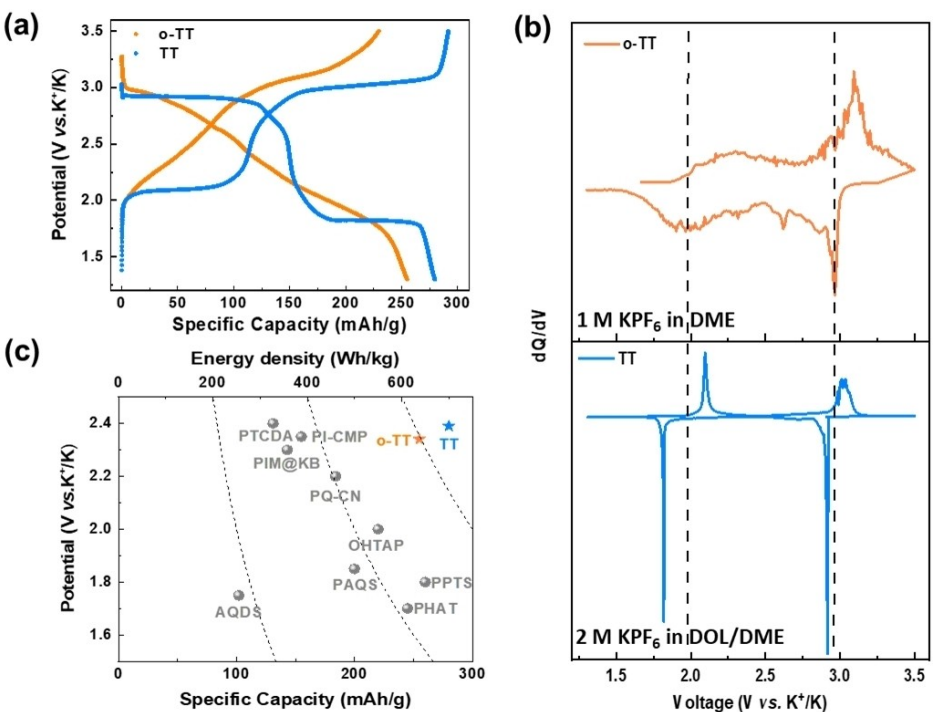


Figure 4. Electrochemical performances of TT and o-TT cathodes in the K coin cells. a) The initial galvanostatic charge/discharge profiles at a 0.1 C-rate in each optimized electrolyte, and b) the corresponding differential capacity curves. c) The plot of average voltage vs. specific capacity with the specific energy of reported n-type organic cathodes in K cells.

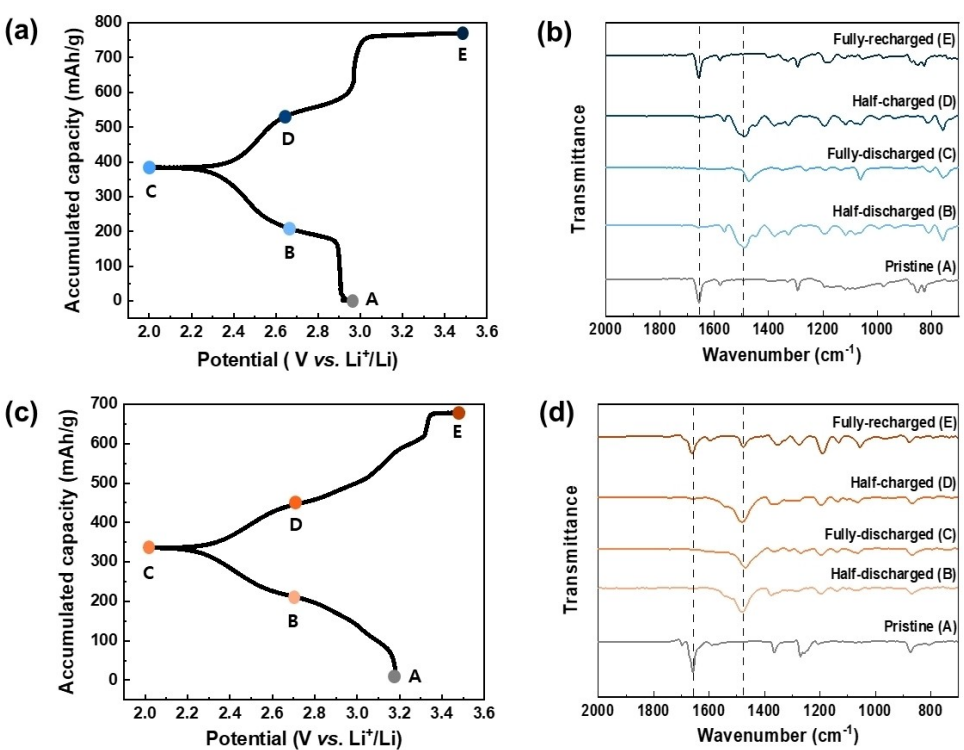


Figure 5. The ex-situ FT-IR spectra of a, b) TT and c, d) o-TT at five different states-of-charge (SOCs) with the corresponding charge/discharge profiles in the Li cells.

Then, by recharge process, the C–O–Li peak of the two TT derivatives is attenuated while their original carbonyl peak arises again in the FT-IR spectra (see point D in Figure 5).

Finally, in the fully recharged state (see point E in Figure 5), the C–O–Li peak of TT disappears completely, indicating its reversible charge/discharge process. In contrast, the enolate peak of o-TT still remains in the fully recharged state. But, in the CV measurement, its redox waves show no changes for 20 cycles, implying the occurrence of reversible redox reactions (See Figure S10). Thus, the remaining peak is most likely ascribed to the formation of solid electrolyte interphase (SEI).^[29]

As in the Li cells, it should be noted that the two TT derivatives show virtually identical changes in the ex-situ FT-IR spectra during the charge/discharge process in the Na and K cells (see Figures S11 and S12).

The peaks in the range of 1000–1400 cm⁻¹ show some changes, corresponding to the vibration of carbon–carbon single bonds, double bonds and their synergistic effects from the six-membered carbon rings.^[30] However, because they consist of numerous complex peaks and also include the signals from PVDF and Super P carbon, it is hard to analyze the changes of the peaks in that range.

Fabrication of disordered mesoporous carbon (DOMC) composites

Despite the large specific capacities of the two TT derivatives at the initial cycle, they showed rapid capacity fading in the subsequent cycles due to the dissolution of active materials into the liquid electrolyte. In the previous research, the cycle stability of TT was considerably improved by fabricating composite materials with ordered mesoporous carbon CMK-3.^[17] In this study, we also fabricated an o-TT/CMK-3 composite electrode with a mixing ratio of 1:2, which was the optimized ratio for TT in the previous study, to improve the cycle stability of o-TT. However, compared to the pristine o-TT electrode, a significantly lowered capacity (< 200 mAh g⁻¹) was utilized from the composite electrode, despite the improved cycle stability (see Figure S13).

As the TT derivatives have a large 3-D molecular structure, we anticipated that the pore size and volume of the mesoporous carbon would be critical for the electrochemical performance of the composite electrodes. Recently, Park et al. reported that the pore volume of the disordered mesoporous carbon (DOMC) was the most critical factor in determining the capacity utilization of a sulfur composite cathode in Li–S cells.^[31] DOMC has a larger pore size (5–10 nm) and volume (2–2.5 cm³ g⁻¹) than CMK-3 (pore size = 3.8–4.0 nm and volume = 1.2–1.5 cm³ g⁻¹), which can facilitate easy access of the metal ions to the infiltrated organic materials inside the carbons. Therefore, we fabricated two composite electrodes of o-TT and DOMC with different mixing ratios of o-TT: DOMC = 1:1 and 1:2, respectively.

The SEM images (Figure S14a) show that DOMC has coarse surfaces, most likely due to many pores. In contrast, DOMC in the two composites has smoother surfaces. Interestingly, while

the SEM image of the 1:1 composite shows aggregated o-TT molecules with the size of a few micrometers outside the DOMC, only Super-P carbon black exists in the 1:2 composite (Figure S14). It clearly indicates that all o-TT molecules are well infiltrated into the pores of DOMC in the 1:2 composite electrode. As expected, the two composite electrodes deliver specific capacities of ~260 mAh g⁻¹, which are comparable to that of the pristine o-TT electrode (~285 mAh g⁻¹) at 1 C-rate in the Li cells. But the 1:2 composite electrode presents better cycle stability than the 1:1 composite in the Li cells (Figure S15). Therefore, the 1:2 composite was used to further evaluate the cycle stability of o-TT and TT in the metal cells (see Figures S16 and S17 for the TT/DOMC composites in the Li cells).

In contrast to the pristine TT and o-TT electrodes, the DOMC composite electrodes show rather slopy charge/discharge profiles in each metal cell (Figures S18 and S19). Because DOMC itself delivers a non-negligible specific capacity (Figures S20 and S21), the capacity contributions from DOMC in the composite electrodes were subtracted from the originally measured specific capacities of the composite electrodes for fair comparisons. As shown in Figure 6, the DOMC composite electrodes exhibit considerably improved cycle stability than the pristine TT and o-TT electrodes in every metal cell. The pristine TT and o-TT electrodes deliver negligible specific capacities after 100 cycles at 1 C-rate. In contrast, the TT/DOMC composite retains 61%, 48%, and 52% of its initial specific capacities in the Li, Na, and K cells, respectively. The o-TT/DOMC composite also maintains 44%, 29%, and 54% of the initial capacities in the Li, Na, and K cells, respectively. Such improved capacity retention of the composite electrodes is attributed to the mesoporous carbon frameworks effectively retarding the dissolution of the infiltrated TT derivatives inside the pores. All DOMC composites show gradual capacity decay or stable cycling after the initial capacity drop, except the TT/DOMC composite in the K cell. Interestingly, as shown in Figure 6(c), the capacity of TT/DOMC in the K cell gradually increases after the initial drop. Such delayed activation of TT is most likely attributed to that the large-size K-ion is difficult to penetrate deeply inside the pores of DOMC. Thus, after the initial capacity drop caused by the dissolution of TT, the non-reacted TT in the deep inside the DOMC might be gradually activated.

Conclusion

In this study, we compared the electrochemical properties of the two triptycene-based isomeric molecules, TT and o-TT, bearing three *para*- or *ortho*-benzoquinones, respectively. The two derivatives showed five single-electron redox reactions in the CV measurements, but the redox reactions of o-TT occurred at higher voltages than TT, as predicted by the DFT calculations.

Then, we evaluated their electrochemical performances as cathode materials in various alkali metal cells, including Li, Na, and K cells. The differential capacity analysis revealed that the

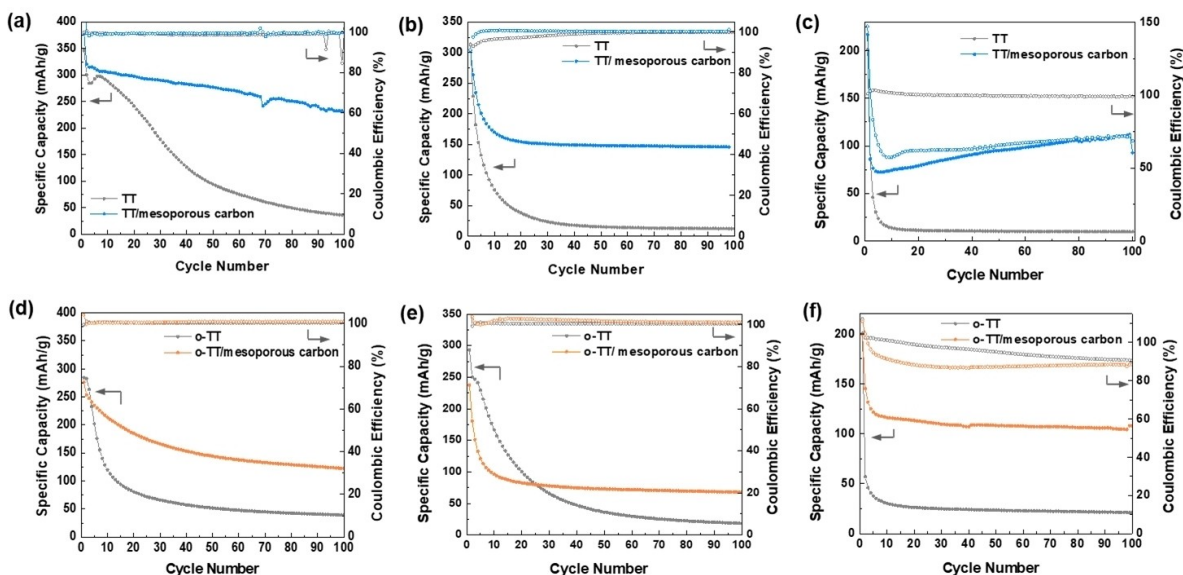


Figure 6. The cycle stability of the TT derivatives and their composites with DOMC at 1 C-rate in a, d) Li, b, e) Na, and c, f) K cells. The upper panels are for TT and the lower ones are for o-TT, respectively.

o-TT electrode showed higher charge/discharge peak voltages than the TT electrode in every metal cell. However, *o*-TT displayed rather slopy charge/discharge profiles, particularly in the Na and K cells, lowering its average charge/discharge voltages and consequently leading to lower specific energies than TT. Nevertheless, it should be noted that, with the aid of large specific capacities coming from the five-electron redox, the two TT derivatives could provide high specific energies exceeding most n-type organic electrode materials in the alkali metal cells. Specifically, the TT electrode delivered energy densities of 1031, 818, and 669 Wh kg⁻¹, while the *o*-TT electrode provided energy densities of 945, 767, and 597 Wh kg⁻¹ in the Li, the Na, and the K cells, respectively. Through this study, it could be learned that, in designing high energy organic electrode materials, not only FMO energies but also other factors such as cation binding, phase transition, and crystallinity changes, should be considered to tune their charge/discharge voltages because the voltage profiles in the bulk electrodes are significantly influenced by those factors.

Through the *ex-situ* FT-IR analyses, their charge/discharge mechanism in the metal cells was clearly elucidated at the molecular scale. The reduction of their carbonyl groups accompanying coordination with the inserted metal ions was responsible for the charge/discharge reaction, which was identical for all alkali metal cells. But, to shed light on the changes of charge/discharge profiles in different metal cells, further investigations for the TT derivatives using crystallography and other spectroscopic methods are desired in future studies.

Finally, we prepared the composite materials of TT and *o*-TT with DOMC nanocarbon to improve their cycle stability. The composite electrodes showed notably improved capacity retention after 100 cycles in the alkali metal cells. However, encapsulating the TT derivatives by the DOMC nanocarbon

could not inhibit their dissolution completely, leading to the gradual capacity fading of the composite electrodes. Furthermore, the DOMC composite electrode exhibited significantly low Coulombic efficiencies in the K cells. Therefore, further studies are desired to improve their performance, including utilizing solid-state electrolytes and polymerization for more practical use.

Nonetheless, this work demonstrated that quinone-based electrode materials could be versatiley applied to diverse metal battery systems with high energy density. Also, the two TT derivatives are expected to be utilized for divalent metal batteries, such as Mg and Zn batteries. Most importantly, we would like to suggest that designing isomers is a simple but effective strategy to elevate the redox voltages of organic electrode materials without sacrificing their specific capacities.

Experimental Section

Materials and general method

All reagents were purchased from commercial suppliers and used without further purification: acetonitrile and dichloromethane (Kanto Chemical Co., inc.), 1,2-Dichloro-5,6-dicyano-1,4-benzoquinone (Tokyo Chemical Industry Co., Ltd.).The NMR spectrum was recorded with a JEOL JNM-A400 instrument. IR spectra were measured on a Perkin Elmer Spectrum One FT-IR Spectrometer in ATR mode. Field emission scanning electron microscopy (FE-SEM) images were acquired using a ZEISS MERLIN Compact with a 2 kV accelerating voltage. The ordered (CMK-3) and disordered mesoporous carbon (DOMC) were purchased from ACS Material and J&K Scientific, respectively.

Synthesis of 9,10-dihydro-9,10-[1,2]benzenoanthracene-2,3,6,7,14,15-hexaone (o-TT)

2,3-Dichloro-5,6-dicyano-1,4-benzoquinone (4.00 g, 17.6 mmol) was added to a suspension of 2,3,6,7,14,15-hexahydroxytryptcene^[32] (1.00 g, 2.85 mmol) in acetonitrile (50 mL), and the mixture was refluxed overnight. The resulting suspension was filtered, washed with acetonitrile (10 mL × 3), and then dried under vacuum to afford brown powder of o-TT (0.780 mg, 79.6%). FTIR(ATR) 3061, 1692, 1657, 1593, 1572, 1365, 1271, 1258, 1205, 1134, 1075, 875, 807, 662 cm⁻¹; ¹H NMR (400 MHz, DMSO-*d*₆) δ (ppm) 6.57(s, 6H), 5.05(s, 2H); ¹³C NMR (400 MHz, DMSO- *d*₆) δ (ppm) 178.8, 147.2, 125.6, 48.1.

Calculations

All density functional theory (DFT) calculations were carried out using the Gaussian 16 quantum-chemical package. The geometry optimizations were performed using (U)B3LYP functionals and the 6-31+G(d,p) basis set. Vibrational frequency calculations were performed for the obtained structures at the same level to confirm the stable minima.

Electrochemical measurements

Cyclic voltammetry (CV) was performed on a Princeton Applied Research Model 273a using a three electrode beaker cell with 0.01 M Ag/AgNO₃ as a reference electrode, a glassy carbon disc as a working electrode, and a platinum wire as a counter electrode, respectively. The reference electrode was calibrated using ferrocene/ferrocenium (Fc⁺/Fc) as an internal standard (Fc⁺/Fc = 0.14 V vs. Ag⁺/Ag). All CV measurements were carried out in a dimethylformamide (DMF) solution containing 5 mM of the quinones with 0.1 M tetrabutylammonium hexafluorophosphate (98%, TCI) as a supporting electrolyte. The scan rate for the measurements was 50 mV s⁻¹.

Preparation of o-TT composites DOMC

The o-TT composites with DOMC were prepared using a simple evaporation method. First, o-TT and DOMC were dissolved in dimethylformamide (DMF). The mixing ratios of o-TT and DOMC in the solutions were 1:1 and 1:2 by weight, respectively. After ultrasonication for 1 h, the solvent of the solutions was slowly evaporated under ambient conditions. The solid mixtures were then placed in a vacuum oven to remove the residual solvents completely.

Cathode fabrication and cell test

The organic cathodes were prepared by blending TT or o-TT with carbon black (Timcal Super P) and polyvinylidene fluoride (PVDF, Sigma Aldrich) in a ratio of 6:3:1 by weight in N-methyl-2-pyrrolidone (NMP) for TT or dimethylformamide (DMF) for o-TT to form a well-dispersed slurry, which was subjected to ultrasonication for 1 h. The slurries were stirred overnight at room temperature and then cast on aluminum foils by doctor blading. The electrodes were dried at 120 °C for NMP or at 30 °C for DMF, respectively, for 8 h in a vacuum oven and then punched into circular discs with a diameter of 14 mm. The typical loading of the TT derivatives and the TT derivatives/DOMC composite were in the range of 1.0–1.3 and 1.3–1.9 mg cm⁻², respectively. Coin type CR2032 (Hohsen) cells were assembled with the cathode and a metal foil anode in an Ar-filled glove box (Korea Kiyon KK-011-AS) in which moisture and oxygen levels were tightly regulated under

0.5 ppm. As a separator, a polypropylene film (Celgard 2400) was used for the Li cells, but glass microfiber filter membrane (Whatman) was used for the Na and K cells. The galvanostatic discharge/charge tests of the coin cells at different current densities were performed on a battery cycler (Wonatech WBCS3000 L) at 30 °C.

Ex-situ analysis of cathodes

The ex-situ samples were prepared at five different states of charge (as-prepared (pristine), half-discharged, fully discharged, half-charged, and fully charged). To prevent contamination by exposure to air, all the samples were moved to an Ar-filled glove box before opening the coin cells. After disassembling the coin cells, the electrodes were washed three times with 1 mL of DME to remove the residual electrolyte salts. Subsequently, the residual solvents were removed from the electrode in a vacuum chamber. Fourier-transform infrared (FT-IR) spectroscopy measurements were conducted using a Nicolet 6700 (Thermo Scientific) with an attenuated total reflectance (ATR) Ge crystal.

Acknowledgements

H. P. and Y. S. contributed equally to this work. This work was supported by Presidential Post-Doc. Fellowship Program through the National Research Foundation (NRF) of Korea (2016R1A6A3A04008134), Korea Institute of Science and Technology (KIST, Korea) Institutional Program (2Z06691 and 2Z06703), and Japan Society for the Promotion of Science (JSPS) KAKENHI Grant (19K15520 and 20H05621).

Conflict of Interest

The authors declare no conflict of interest.

Data Availability Statement

The data that support the findings of this study are available from the corresponding author upon reasonable request.

Keywords: alkali metal batteries • electrochemistry • isomers • organic electrode materials • quinones

- [1] a) V. Etacheri, R. Marom, R. Elazari, G. Salitra, D. Aurbach, *Energy Environ. Sci.* 2011, 4, 3243–3262; b) P. Poizot, J. Gaubicher, S. Renault, L. Dubois, Y. Liang, Y. Yao, *Chem. Rev.* 2020, 120, 6490–6557.
- [2] a) T. B. Schon, B. T. McAllister, P. F. Li, D. S. Seferos, *Chem. Soc. Rev.* 2016, 45, 6345–6404; b) Y. Guo, H. Li, T. Zhai, *Adv. Mater.* 2017, 29, 1700007; c) G. E. Blomgren, *J. Electrochem. Soc.* 2016, 164, A5019–A5025.
- [3] a) M. D. Slater, D. Kim, E. Lee, C. S. Johnson, *Adv. Funct. Mater.* 2013, 23, 947–958; b) J. Y. Hwang, S. T. Myung, Y. K. Sun, *Chem. Soc. Rev.* 2017, 46, 3529–3614.
- [4] H. Wang, D. Yu, C. Kuang, L. Cheng, W. Li, X. Feng, Z. Zhang, X. Zhang, Y. Zhang, *Chem* 2019, 5, 313–338.
- [5] a) R. Rajagopalan, Y. Tang, X. Ji, C. Jia, H. Wang, *Adv. Funct. Mater.* 2020, 30, 1909486; b) L. Li, Y. Zheng, S. Zhang, J. Yang, Z. Shao, Z. Guo, *Energy Environ. Sci.* 2018, 11, 2310–2340.

- [6] H. Kim, D. H. Seo, J. C. Kim, S. H. Bo, L. Liu, T. Shi, G. Ceder, *Adv. Mater.* **2017**, *29*, 170248.
- [7] Y. Lu, Q. Zhang, L. Li, Z. Niu, J. Chen, *Chem* **2018**, *4*, 2786–2813.
- [8] a) Y. Wu, R. Zeng, J. Nan, D. Shu, Y. Qiu, S.-L. Chou, *Adv. Energy Mater.* **2017**, *7*, 1700278; b) Q. Zhao, Y. Lu, J. Chen, *Adv. Energy Mater.* **2017**, *7*, 1601792; c) H. Peng, Q. Yu, S. Wang, J. Kim, A. E. Rowan, A. K. Nanjundan, Y. Yamauchi, J. Yu, *Adv. Sci.* **2019**, *6*, 1900431.
- [9] a) W. Huang, Z. Zhu, L. Wang, S. Wang, H. Li, Z. Tao, J. Shi, L. Guan, J. Chen, *Angew. Chem. Int. Ed. Engl.* **2013**, *52*, 9162–9166; b) Z. Zhu, M. Hong, D. Guo, J. Shi, Z. Tao, J. Chen, *J. Am. Chem. Soc.* **2014**, *136*, 16461–16464.
- [10] a) S. Zheng, J. Hu, W. Huang, *Inorg. Chem. Front.* **2017**, *4*, 1806–1812; b) W. Xiong, W. Huang, M. Zhang, P. Hu, H. Cui, Q. Zhang, *Chem. Mater.* **2019**, *31*, 8069–8075.
- [11] Z. Jian, Y. Liang, I. A. Rodríguez-Pérez, Y. Yao, X. Ji, *Electrochim. Commun.* **2016**, *71*, 5–8.
- [12] Z. Song, H. Zhan, Y. Zhou, *Chem. Commun.* **2009**, 448–450.
- [13] a) T. Yokoji, H. Matsubara, M. Satoh, *J. Mater. Chem. A* **2014**, *2*, 19347–19354; b) H. Banda, D. Damien, K. Nagarajan, A. Raj, M. Hariharan, M. M. Shajumon, *Adv. Energy Mater.* **2017**, *7*, 1701316; c) H. Kim, J. E. Kwon, B. Lee, J. Hong, M. Lee, S. Y. Park, K. Kang, *Chem. Mater.* **2015**, *27*, 7258–7264.
- [14] a) Y. Liang, P. Zhang, S. Yang, Z. Tao, J. Chen, *Adv. Energy Mater.* **2013**, *3*, 600–605; b) B. Zhang, Y. Zhang, X. Yang, G. Li, S. Zhang, Y. Zhang, D. Yu, Z. Liu, G. He, *Chem. Mater.* **2020**, *32*, 10575–10583; c) A. Iordache, V. Maurel, J.-M. Mouesca, J. Pécaut, L. Dubois, T. Gutel, *J. Power Sources* **2014**, *267*, 553–559.
- [15] S. Gottis, A. L. Barres, F. Dolhem, P. Poizot, *ACS Appl. Mater. Interfaces* **2014**, *6*, 10870–10876.
- [16] L. Miao, L. Liu, Z. Shang, Y. Li, Y. Lu, F. Cheng, J. Chen, *Phys. Chem. Chem. Phys.* **2018**, *20*, 13478–13484.
- [17] J. E. Kwon, C.-S. Hyun, Y. J. Ryu, J. Lee, D. J. Min, M. J. Park, B.-K. An, S. Y. Park, *J. Mater. Chem. A* **2018**, *6*, 3134–3140.
- [18] Y. Shuku, A. Mizuno, R. Ushiroguchi, C. S. Hyun, Y. J. Ryu, B. K. An, J. E. Kwon, S. Y. Park, M. Tsuchii, K. Awaga, *Chem. Commun.* **2018**, *54*, 3815–3818.
- [19] Y. Ryu, C.-S. Hyun, B.-K. An, *Synth. Commun.* **2022**, *52*, 1184–1189.
- [20] S. Langis-Barsetti, T. Maris, J. D. Wuest, *J. Org. Chem.* **2018**, *83*, 15426–15437.
- [21] A. Kuhn, K. G. von Eschwege, J. Conradie, *J. Phys. Org. Chem.* **2012**, *25*, 58–68.
- [22] N. Nagamura, R. Taniki, Y. Kitada, A. Masuda, H. Kobayashi, N. Oka, I. Honma, *ACS Appl. Energ. Mater.* **2018**, *1*, 3084–3092.
- [23] C. O. Laoire, E. Plichta, M. Hendrickson, S. Mukerjee, K. Abraham, *Electrochim. Acta* **2009**, *54*, 6560–6564.
- [24] L. Lutz, D. Alves Dalla Corte, M. Tang, E. Salager, M. Deschamps, A. Grimaud, L. Johnson, P. G. Bruce, J.-M. Tarascon, *Chem. Mater.* **017**, *29*, 6066–6075.
- [25] a) K. Zhang, C. Guo, Q. Zhao, Z. Niu, J. Chen, *Adv. Sci.* **2015**, *2*, 1500018; b) T. Ma, Q. Zhao, J. Wang, Z. Pan, J. Chen, *Angew. Chem. Int. Ed. Engl.* **2016**, *55*, 6428–6432.
- [26] J. Park, J. Lee, M. H. Alfaruqi, W.-J. Kwak, J. Kim, J.-Y. Hwang, *J. Mater. Chem. A* **2020**, *8*, 16718–16737.
- [27] a) M. Tang, Y. Wu, Y. Chen, C. Jiang, S. Zhu, S. Zhuo, C. Wang, *J. Mater. Chem. A* **2019**, *7*, 486–492; b) R. R. Kapaev, I. S. Zhidkov, E. Z. Kurmaev, K. J. Stevenson, P. A. Troshin, *J. Mater. Chem. A* **2019**, *7*, 22596–22603.
- [28] a) J. Yang, P. Xiong, Y. Shi, P. Sun, Z. Wang, Z. Chen, Y. Xu, *Adv. Funct. Mater.* **2020**, *30*, 1909597; b) S. Zhang, Y. Zhu, D. Wang, C. Li, Y. Han, Z. Shi, S. Feng, *Adv. Sci.* **2022**, *9*, e2200397.
- [29] a) W. Luo, M. Allen, V. Raju, X. Ji, *Adv. Energy Mater.* **2014**, *4*, 1400554; b) Y. Liu, X. Zhao, C. Fang, Z. Ye, Y.-B. He, D. Lei, J. Yang, Y. Zhang, Y. Li, Q. Liu, Y. Huang, R. Zeng, L. Kang, J. Liu, Y.-H. Huang, *Chem* **2018**, *4*, 2463–2478; c) M. Zhou, M. Liu, J. Wang, T. Gu, B. Huang, W. Wang, K. Wang, S. Cheng, K. Jiang, *Chem. Commun.* **2019**, *55*, 6054–6057.
- [30] a) Z. Lin, H.-Y. Shi, L. Lin, X. Yang, W. Wu, X. Sun, *Nat. Commun.* **2021**, *12*, 1–9; b) H. Makita, G. Hastings, *Biochim. Biophys. Acta Bioenerg.* **2020**, *1861*, 148173; c) J.-R. Burie, A. Boussac, C. Boulleau, G. Berger, T. Mattioli, C. Mioskowski, E. Nabedryk, J. Breton, *J. Phys. Chem.* **1995**, *99*, 4059–4070.
- [31] M.-S. Park, B. O. Jeong, T. J. Kim, S. Kim, K. J. Kim, J.-S. Yu, Y. Jung, Y.-J. Kim, *Carbon* **2014**, *68*, 265–272.
- [32] B. S. Ghanem, M. Hashem, K. D. M. Harris, K. J. Msayib, M. Xu, P. M. Budd, N. Chaukura, D. Book, S. Tedds, A. Walton, N. B. McKeown, *Macromolecules* **2010**, *43*, 5287–5294.

Manuscript received: November 14, 2022

Revised manuscript received: December 22, 2022

Accepted manuscript online: December 25, 2022

Version of record online: January 10, 2023